

Computation of conventional and alternative jet fuel sensitivity to lean blowout

Veeraraghava Raju Hasti^{a,*}, Prithwish Kundu^b, Sibendu Som^b, Sang Hee Won^c, Frederick L. Dryer^c, Jay P. Gore^a

^a School of Mechanical Engineering, Purdue University, West Lafayette, IN, 47907, USA

^b Argonne National Laboratory, Argonne, Illinois, 60439, USA

^c University of South Carolina, Columbia, SC, 29208, USA

ARTICLE INFO

Keywords:

Large eddy simulation
Lean blowout
Gas turbine combustor
Alternative aviation fuel
Adaptive mesh refinement
Chemical kinetics
Reaction mechanism

ABSTRACT

Large Eddy Simulations (LES) are performed to compute the sensitivity of a conventional (A-2) and an alternate bio-jet (C-1) fuel to Lean Blowout (LBO). A realistic aviation gas turbine engine combustor configuration is considered. Reliable experimental LBO data and OH* chemiluminescence data for the conventional and alternate jet fuel in the combustor configuration have recently become available. The present work utilizes a highly automated, on-the-fly meshing strategy, along with adaptive mesh refinement, to demonstrate the feasibility of capturing the realistic combustion processes. A Lagrangian framework, with initial conditions specified using measurements of spray statistics, is used to model the fuel spray. Newly developed compact reaction mechanisms based on fuel surrogates are validated for the A-2 and the C-1 fuels. The compact reaction mechanisms are implemented using a detailed finite rate chemistry solver. Spray statistics computed by the present LES simulations compare well with available measurements at stable flame conditions near the lean blowout limit. The computed shape of the stable flame as represented by line integrated OH concentrations compares well with the experimental OH* chemiluminescence data. Lean blowout is reached by gradually decreasing the fuel flow rate in the computations, similar to that in the experiments. The results of the LES simulations effectively capture the fuel composition effects and estimate the sensitivity of the LBO limits to the fuel type. The computed trends in LBO limits agree within engineering accuracy with the experimental results for conventional and alternative aviation fuels. The methodology for predicting the fuel composition effects on the lean blowout limits in a fully resolved realistic, complex combustor is established for the first time.

1. Introduction

Environmental policies and restrictions aimed at reducing the use of petroleum-derived fuels and resulting emissions have motivated recent research into alternate bio-liquid aviation fuels. The main figures of merit for certification of aviation fuels are cold start, high altitude relight (HAR), and lean blowout (LBO). The performance of conventional and renewable fuels with respect to lean blowout, high altitude relight, and pollutant emission is being measured at many laboratories around the world. Within the USA, the National Jet Fuel Combustion Program (NJFCP) represents a multi-agency collaboration aimed at streamlining the fuel certification procedures for alternative jet fuels [1, 2]. The experiments under the NJFCP program utilize a single cup realistic gas turbine combustor called the Air Force Research Laboratory

(AFRL) referee combustor. The referee combustor has been operated under numerous operating conditions to determine the lean blowout (LBO) and ignition characteristics of alternative and petroleum-derived fuels [1–6]. Measurements for spray and flame characteristics at engine-relevant conditions in the referee combustor are reported in the literature [3,4,6–11]. Three petroleum-derived jet fuels (A-1 to A-3) and several bio-derived jet fuels have been investigated in the NJFCP program to evaluate the effects of physical and chemical properties. A-2 fuel represents the global norm for petroleum-derived jet fuels, while C-1 is a bio-derived alternative jet fuel consisting of two specific iso-paraffins, iso-cetane and 2,2,4,6,6-pentamethylheptane (iso-dodecane). Further description for A-2 and C-1 fuels with properties is given in Ref. [12].

Stouffer et al. [4] studied the LBO and ignition characteristics of eight fuels in a referee combustor through experiments. The data

* Corresponding author. 585, Purdue Mall, West Lafayette, IN, 47907, USA.

E-mail address: vhasti@purdue.edu (V.R. Hasti).

showed that higher derived cetane number (DCN) fuels result in a broader range of operability. Lieuwen et al. [13] experimentally studied the effects of fuel composition on LBO, flashback, and ignition for a syngas-fueled combustor. The results showed that higher hydrogen content in fuels leads to a lower lean blowout limit. Stöhr et al. [14] experimentally studied the dynamics of LBO in a methane-fueled gas turbine combustor at atmospheric pressure using OH- planar laser-induced fluorescence (PLIF), chemiluminescence imaging, and stereo particle imaging velocimetry (SPIV). Their results show that localized extinction events near the flame root initiate because of high strain rates. The continuation of the localized flame extinction events, over time, leads to global flame extinction (i.e., LBO).

Esclapez et al. [15] computed the fuel sensitivity to LBO in the referee combustor using an incompressible flow solver (VIDA) and large eddy simulations (LES). The combustor liners are simplified, and effusion cooling is modeled using homogeneous boundary conditions with specified mass flow rates. A flamelet progress variable (FPV) combustion model and a WALE subgrid-scale turbulence model were used. The HyChem kinetic mechanisms [16–19] were used to model the fuel chemistry. The simulation results for a stable condition near LBO for flame shape and spray characteristics (droplet axial and radial velocity, Sauter Mean Diameter (SMD)) qualitatively agree with experimental data. However, LBO trends from simulations are opposite to the experimental results for A-2 and C-1 fuels. The complex combustion behavior, especially during the LBO process, results from the transient three-dimensional flow field involving complex multiscale mixing, mass transfer, heat transfer, and multistep reaction processes. The numerical simulations of these processes must be multidimensional and multiscale utilizing multiple sub-models with limited assumptions. The kinetic mechanisms with a large number of species and reactions are required for capturing the heat release rates and especially the competing rates of multiple reactions necessary for maintenance of a radical pool. Literature on simulations for predicting the fuel sensitivity to LBO limits in a fully resolved realistic combustor geometry with detailed chemistry is limited and warrants further research to develop high fidelity computational modeling approach.

The objective of the present work is to develop high-fidelity LES simulations of a practical combustor geometry to fully resolve the complex processes affecting the fuel sensitivity to LBO of A-2 and C-1 fuels. This work demonstrates a holistic modeling approach starting from 1) inclusion of as-it-is features of the practical combustor hardware in the computational domain, 2) resolving flow through all complex passages within the combustor, 3) comprehensive fuel spray definition using a multi-ring annulus with spray measurements for prescription of the initial conditions, 4) target fuel property characterization, 5) kinetic mechanism development using a surrogate formulation based on combustion property targets, and 6) optimization of the compact chemical kinetic model against detailed model prediction, 7) implementation of kinetic mechanisms in CFD, 8) multidimensional LES simulations to capture the experimentally observed LBO behaviors, 9) validation with experiments. The computational methodology utilized autonomous and adaptive meshing and refinement and a comprehensive finite rate chemistry solver with detailed chemical kinetics. New kinetic mechanisms based on combustion property target surrogate mixture emulation of A-2 [20–23] and C-1 fuels [23,24] were developed, validated, and implemented in this study. These mechanisms were successfully utilized for the first time in CFD for LBO computations.

The rest of this paper is organized as follows. Section 2 describes the computational model. Section 3 provides details of the development and validation of the chemical kinetic mechanisms. Section 4 includes a presentation and discussion of the computational results, comparison with experiments, and characterization of the combustion zones. Finally, Section 5 includes a summary of the results, conclusions, and recommendations for future work.

2. Computational model

LES simulations of liquid fuel combustion in the referee combustor were performed utilizing a multiphase, multispecies, finite volume-based compressible flow solver CONVERGE [25]. The Eulerian approach is used to solve the continuous gas phase equations, and the Lagrangian approach is used to model the liquid spray with discrete injections of droplets. The compressible form of the Favre-averaged Navier-Stokes equations, species transport equations, energy equation, and the equation of state are solved on a non-staggered, collocated computational grid. The dynamic structure sub-grid scale model [26,27] is used for turbulence. A detailed finite rate chemistry solver is employed for combustion along with a well-stirred reactor (WSR) model for the sub-grid scale turbulence chemistry interactions. The finite rate chemistry solver with a detailed chemical kinetic mechanism can model the non-premixed, premixed, and partially premixed combustion. This approach can accurately compute strong finite rate chemistry effects during local extinction/re-ignition events in the initiation phase and during local and global flame extinction. Use of the WSR sub-grid scale model on a sufficiently resolved grid adapted in this work has been demonstrated in the literature for computations of combustion processes in engines [28–33].

Fig. 1 shows the details of the referee combustor within the present 3D CFD domain. The complex flow passages on the practical combustor liners are fully resolved. These passages include thousands of tiny effusion holes, film cooling holes, two rows of dilution holes, and hybrid air blast swirler passages. The annulus airflow through the cooling holes (aft slot holes and window effusion) at the combustor exit are not designed to participate in the combustion process. Therefore, these passages are not included in the CFD domain. The total air mass flow rate is prescribed to be 338.7 g/s (excluding the window and aft slot cooling flow) at an inlet temperature of 394 K with a specified value (from the measurements close to the combustor exit) of the static pressure boundary condition at the combustor exit. The Werner and Wengle wall model [34] is prescribed for the velocity boundary conditions. The adiabatic boundary condition is used for all the combustor walls.

The Phase Doppler Particle Analyzer (PDPA) measurements from Refs. [7,9,10] for the fuel injector at the non-reacting conditions corresponding to the stable flame near LBO are utilized to generate the initial conditions for the present simulations. The PDPA measurements are taken at a distance of 25.4 mm from the deflector plate (shown with blue color in Fig. 1). The measurements are projected upstream to define the spray boundary condition as an ensemble of six ring injectors at a distance of 2 mm from the exit of the fuel nozzle. The droplet size distribution, velocity, fuel mass flow rate, spray angle, and the number of parcels stipulated as initial conditions for each ring are shown in Fig. 2. Secondary breakup is modeled using the Taylor Analogy Breakup (TAB) model, and the particle drag is computed using the dynamic drag model [25]. The droplet dispersion model [25] is utilized to include the effects of sub-grid scale turbulence on the discrete parcels. The Frossling correlation [35] is utilized to model droplet evaporation. The fuel properties for the A-2 and C-1 fuel from the NJFCP database are utilized [12].

The LES simulations utilize autonomous meshing with the Cartesian cut cell method [36]. The complex passages of the combustor hardware are modeled and gridded to compute the reacting flow field accurately. The technique automatically generates the mesh on the fly during execution by the solver. The grid generation in the computational domain is defined based on the specified base size of the mesh. A priori embedding is fixed to resolve high gradients with a fine mesh in the areas near the fuel injector, the swirl cup, the recirculation zones within the primary zone, the dilution jets, the liner effusion holes, and the film cooling holes. The adaptive mesh refinement (AMR) algorithm is used to refine and coarsen the mesh on the fly based on the temperature, species concentration, and velocity gradients. The AMR optimizes the computational time without compromising the accuracy. Fig. 3 depicts a representative sample of an instantaneous mesh distribution on the

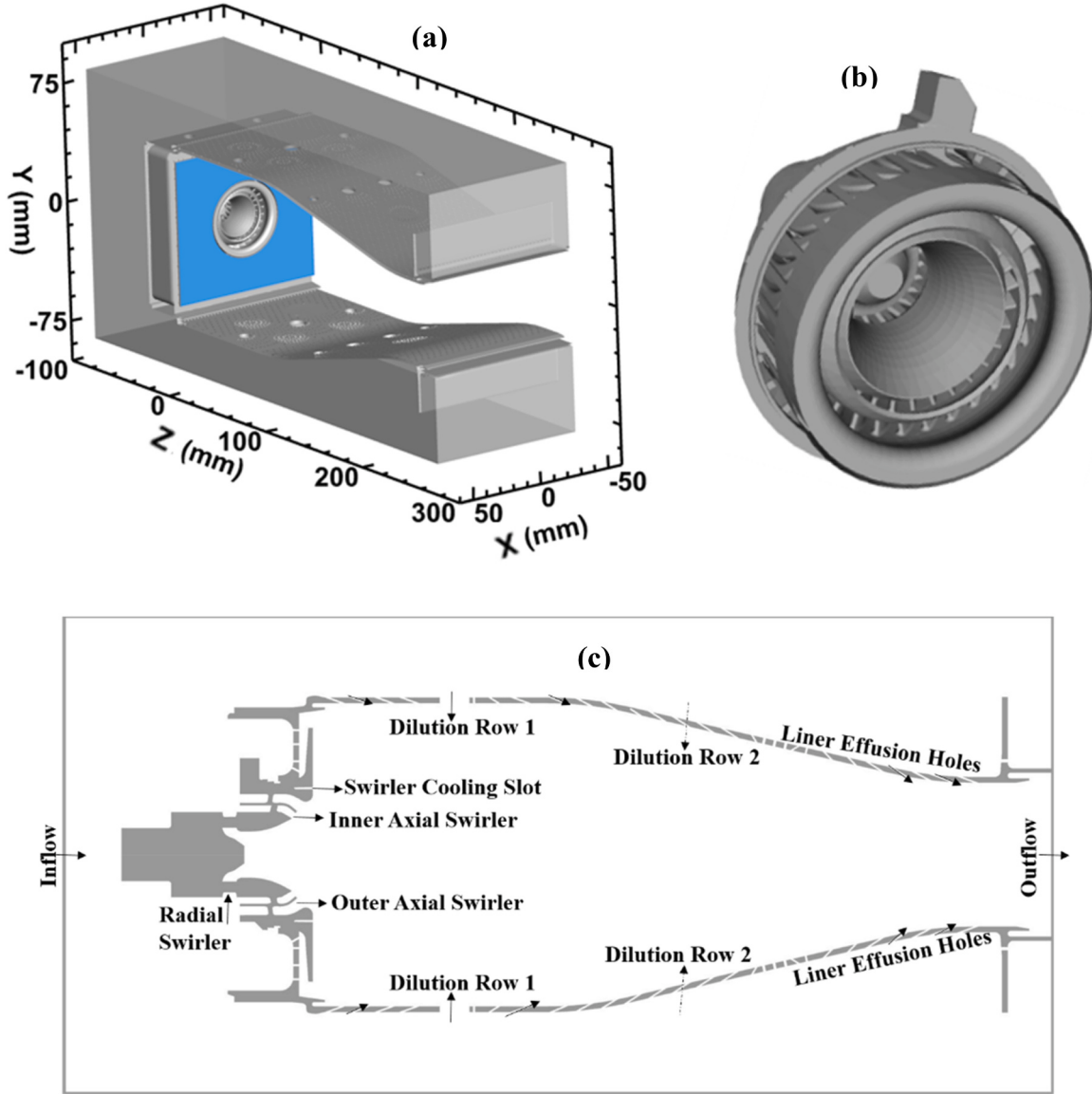


Fig. 1. (a) Referee combustor CFD domain (b) Hybrid air blast swirler magnified view (c) Cross-section of the combustor at $X = 0$.

combustor mid-plane ($X = 0$) resulting from 3 levels of AMR following a base mesh size of 3 mm, a minimum cell size of 0.375 mm, and a total cell count of 10 million.

More than 80% of the turbulent kinetic energy was resolved by the LES mesh parameters resulting from a grid sensitivity study and analysis [37–40]. The independence of the computed lean blowout equivalence ratio from the mesh resolution was established by simulating with two significantly different mesh resolutions. Total cell counts of 10 million with a minimum cell size of 0.375 mm and 25 million with a minimum cell size of 0.1875 mm resulted in a computed global equivalence ratio of 0.092 at lean blowout (LBO). Evaluation of the turbulent kinetic energy with the 10 million mesh illustrates over 90% resolution in the combustor, as shown in Fig. 4. In regions with high turbulence, the resolved scale turbulence kinetic energy reaches values as high as 96%. These regions include the dilution jets, the swirl cup, the recirculation zones, and the shear layers. This mesh distribution satisfies the well-established criteria in the literature for accurate LES simulations [41]. The present autonomous and adaptive meshing strategy and procedures, along with the present detailed finite rate chemistry solver, have been successfully validated in past studies by authors for a wide range of problems [38,39,42–51].

Results of the experiments reported in Ref. [4] show that the near stable flame condition corresponds to a global equivalence ratio of 0.096 before approaching the unstable flame and lean blowout in the referee combustor. Therefore, simulations are first performed for the stable flame condition corresponding to the global equivalence ratio of 0.096. The fuel flow rate is then gradually decreased from this stable condition in a stepwise manner until the LBO equivalence ratio is approached. The volume integrated heat release rate in the combustor is monitored during the simulation for each fuel flow rate. The fuel flow rate for each reduction step is maintained constant in CFD simulations for at least two flow-through times (~30 ms). If a quasi-steady heat release rate is not attained during this time, then simulations are continued beyond 30 ms until a quasi-steady state is reached for heat release rate. The further reduction in the fuel flow rate is terminated once the volume integrated heat release rate approaches zero, thus identifying the lean blowout condition. The LBO simulations are run using the Broadwell nodes on the NASA Pleiades supercomputer. Broadwell node uses E5-2680v4 (2.4 GHz) processors and contains 28 cores with 128 GB memory. The reacting LES simulations on 280 processors for 10 ms took approximately 88 h.

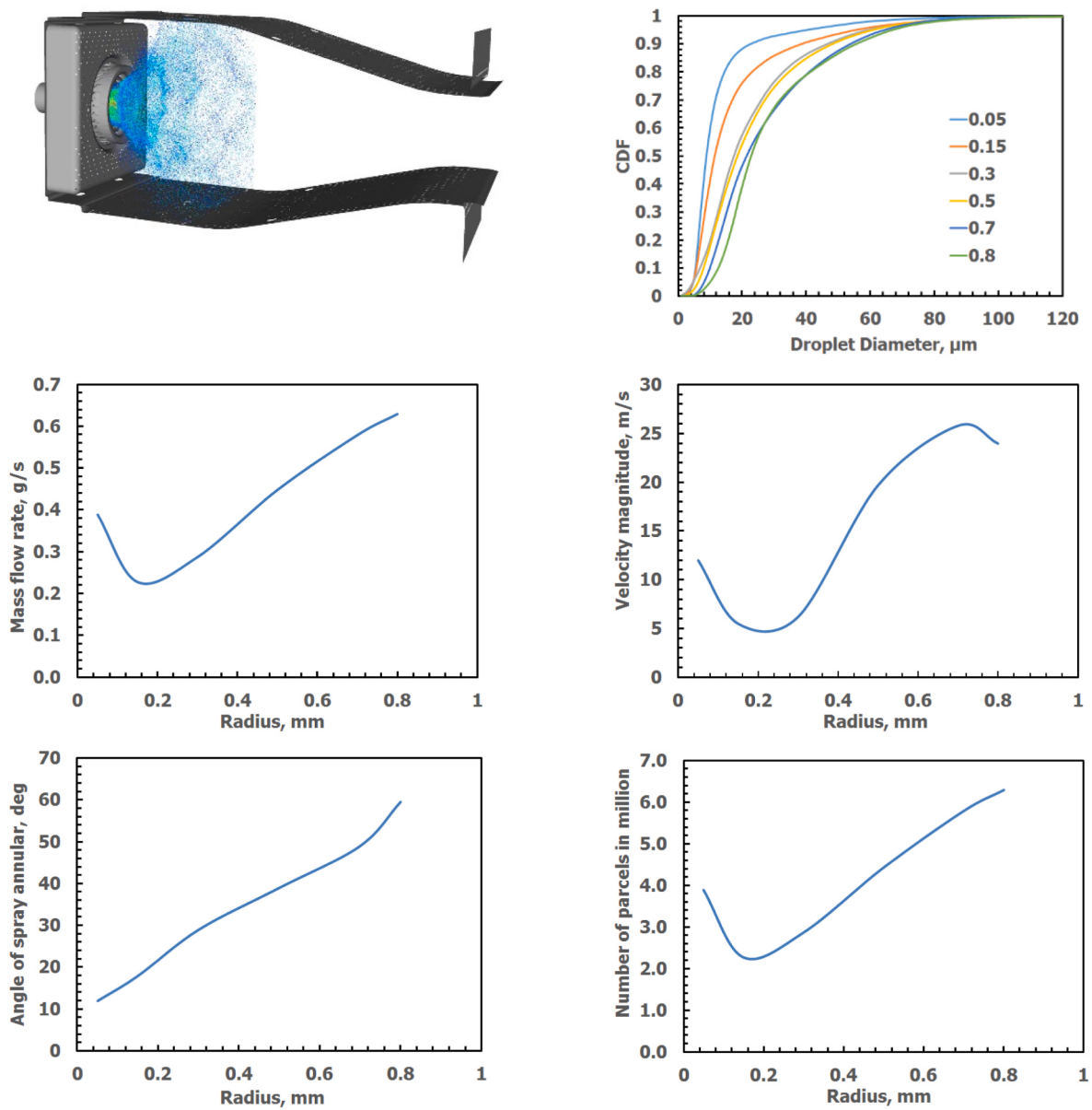


Fig. 2. Spray boundary conditions. CDF is Cumulative Distribution Function.

3. Development of the compact kinetics sub-models

Jet fuels derived from petroleum and alternative sources are complex chemical mixtures that contain numerous hydrocarbon components. Furthermore, the chemical compositions of both petroleum-derived and alternative jet fuels vary considerably [52], thus exhibiting significant variations of combustion behaviors even in fully vaporized conditions (e.g., homogeneous reflected shock ignition delay times, laminar flame speeds, and flame extinction limits) [20–22,53]. A surrogate mixture is a model chemical composition that can emulate some critical fuel properties of a target real fuel. It was previously demonstrated that the fully pre-vaporized combustion behaviors of a target real fuel could be well emulated with the surrogate mixture that was formulated by matching four combustion property targets [52]: hydrogen-to-carbon molar ratio (H/C ratio), derived cetane number (DCN), average molecular weight, and threshold sooting index (TSI).

The surrogate mixture for A-2 (Jet-A POSF 10325) is composed of n-dodecane, iso-octane, and 1,3,5-trimethyl benzene (0.49, 0.21, and 0.30 in mole fraction, respectively) as discussed in Ref. [54] as “surrogate 1”. The surrogate mixture of C-1 (Gevo-ATJ POSF 10151) is formulated

with iso-cetane and iso-octane in equal composition [53,55]. The C-1 fuel is composed of iso-cetane (iC16, ~15% in liquid volume) and iso-dodecane (iC12, 2,2,4,6,6-pentamethylheptane, ~85% in liquid volume) [24,56]. The global combustion characteristics of A-2 and C-1 fuels have already been extensively reported in the literature [53–55].

A compact chemical kinetic model is produced by optimizing the kinetic rate parameters in fuel-chemistry subsets to match the species profiles predicted by a detailed chemical kinetic model. It utilizes the species profiles predicted by a target detailed model over the following range of conditions: initial temperature from 700 to 1800 K, pressures from 1 to 20 atm, and equivalence ratios of 0.6, 1.0, 1.5, and 3.0. Although the potential impacts of preferential vaporization have been reported particularly for LBO behaviors [57,58], a representative single-molecule approach has been taken here to minimize the dimensionality of the compact model. The fuel molecule for A-2 and C-1 is represented by $\text{C}_{11}\text{H}_{22}$ and $\text{C}_{12}\text{H}_{26}$, respectively. As a target detailed chemical kinetic model, RealFuel 3 has been utilized. Details on RealFuel 3 construction and the optimization approach for the compact model can be found in Refs. [46,59], where reasonable emulations of fully pre-vaporized combustion behaviors (ignition delay times and

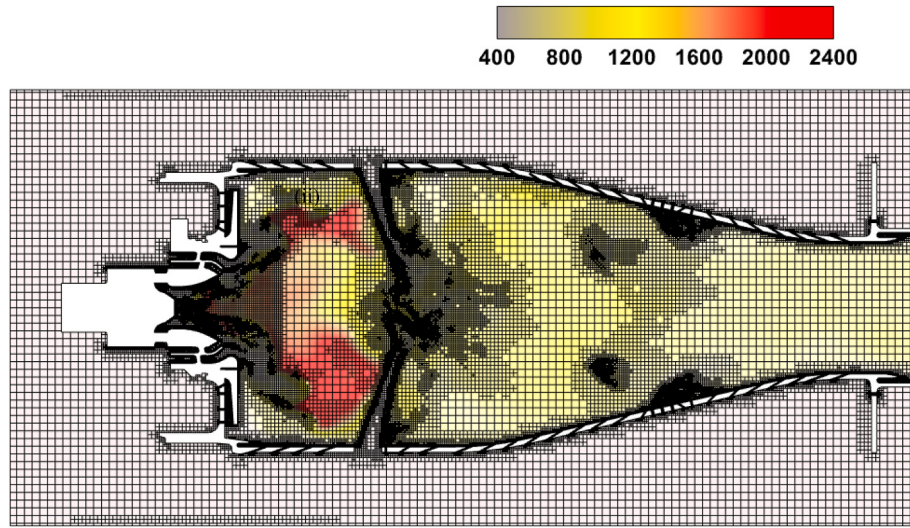


Fig. 3. Computational grid on combustor mid-plane ($X = 0$ plane) with adaptive mesh refinement. Colored with instantaneous temperature.

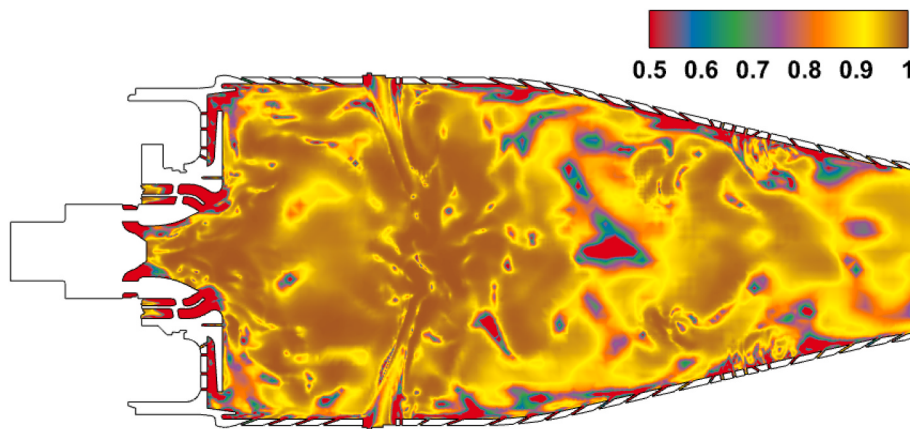


Fig. 4. Fraction of the resolved turbulent kinetic energy (LES resolution).

laminar flame speeds) by the optimized compact model have been reported. The objective of the compact model optimization approach taken here is to produce a compact model that fruitfully emulates the performance of the target detailed model so that any deficiencies found in multidimensional simulation can be related to the potential deficiencies in the original detailed model. The compact model for A-2 contains 44 species and 229 reaction steps, while that of C-1 contains 43 species and 267 reaction steps.

3.1. Evaluation of compact model

Fig. 5 compares the ignition delay times between A-2 and C-1, predicted by compact and detailed models. A-2 (Jet-A POSF 10325) was purposely prepared by US Air Force Research Laboratory (AFRL) to have average values of key fuel properties. As a result, the combustion property targets of A-2 share almost identical values with the previously studied average petroleum-derived jet fuel, Jet-A POSF 4658. Jet-A POSF 4658 was also prepared similarly by AFRL [53]. Therefore, the measured ignition delay times previously reported in Ref. [21] are used to compare the model predictions with the measurements. In the case of C-1, model predictions are compared to the measurement with iso-dodecane (2,2,4,6,6-pentamethylheptane) reported in Ref. [55], based on the similarity of ignition propensities among iso-dodecane and iso-cetane [56].

A comparison between the model predictions and the measurements

of A-2 and C-1 for stoichiometric fuel/air mixtures at 20 atm condition suggests that both detailed and compact chemical kinetic models capture the differences between ignition delay times for both fuels. The optimized compact models reasonably capture these delay times. On the other hand, the detailed model over-predicts the ignition delay times consistently for both A-2 and C-1. Since the LBO experiments were conducted at ~2 atm, the results of the compact model predictions for A-2 and C-1 at 2 atm are depicted in **Fig. 5**. The results show that the ignition delay times of A-2 are slightly faster than those of C-1.

Fig. 6 shows a comparison of laminar flame speeds at 1 atm in a function of equivalence ratio for both A-2 and C-1. Here, the measurements for Jet-A POSF 4658 reported in Dooley et al. [21] and A-2 in Wang et al. [19] are compared to the compact model predictions (solid lines), while the measurements for C-1 reported in Wang et al. [19] are used for the comparison to the model prediction. The predictions by the detailed model are not included in the figure for simplicity. The compact models can accurately reproduce the detailed model's predictions, as reported previously [23,46]. **Fig. 6** also compares the laminar flame speeds at 2 atm predicted by the compact models. In general, the compact models can emulate the qualitative difference between A-2 and C-1, suggesting the higher reactivity of A-2 over C-1.

The two compact kinetic models developed in this work can be successfully utilized in computing the global combustion characteristics for conventional (A-2) and alternative (C-1) jet fuels over a range of operating conditions. It should be highlighted that these models and

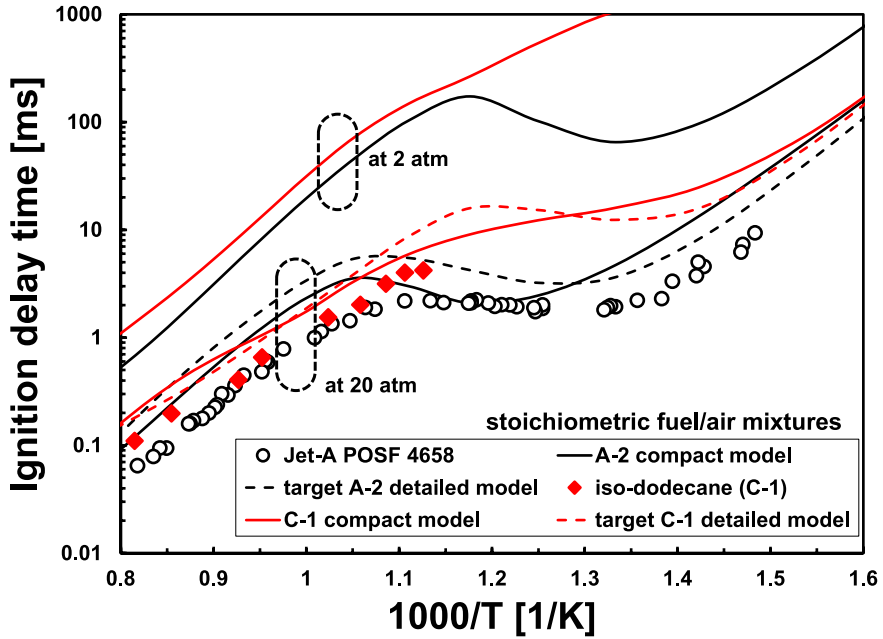


Fig. 5. Measured and predicted ignition delay times for stoichiometric fuel/air mixtures of A-2 and C-1 at 20 atm nominal pressure. Predicted ignition delay time at 2 atm suggests higher reactivity of A-2 over C-1.

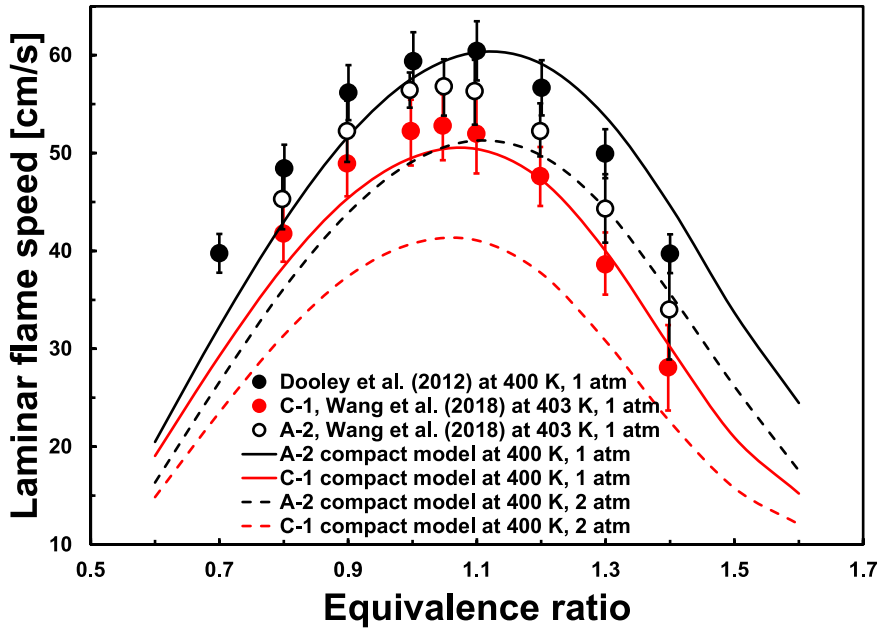


Fig. 6. Measured laminar flame speeds of A-2 and C-1 compared to the predictions by the compact models.

other fuel-specific compact models are produced using basic ASTM standards for fuel property assessments with relatively modest amounts ~ 200 mL, with no requirement of global combustion experiments. Though the availability of such data may be exploited to fine-tune the kinetic model, the predictive fidelity of these models without further optimization is sufficient for computational engineering design applications.

4. Results and discussion

The flow field generated by the complex swirler geometry, the cross

jets, and the liner cooling flows has been computed with a non-reacting flow version of the present computations completed on an identical initial mesh. The results of these computations agree reasonably well with the experimental data, particularly in terms of flow splits, as reported previously [37]. The results of the present simulations for the spray properties and computed flame shape for both the A-2 and the C-1 fuels at the stable flame condition ($\varphi = 0.096$) are first compared with experimental data. These comparisons show that the model captures the trends for the spray properties and flame shapes for the two fuels reasonably well, as discussed in further detail in the following sections.

4.1. Comparison of the LES results with experimental data at the stable flame condition

Flame stability is determined by fuel droplet dynamics and vaporization, fluid dynamic mixing, localized extinction, re-ignition, and various other dynamically coupled processes. The local fuel-air distribution resulting from spray penetration, local evaporation rates for droplets, droplet size distribution, and molecular and turbulent mixing affect the local extinction process. With a variety of atomizer designs and operating conditions, droplet size distribution and preferential vaporization of fuel components are also relevant processes. Appropriate drop size and velocity distributions are important for achieving the desired pattern factor, emissions, combustion efficiency, and operability characteristics. The results of the spray modeling are therefore assessed first, considering their important role in successful simulations of liquid fuel combustion and flame stability.

The statistics for the spray properties from LES simulations at the near stable flame condition ($\varphi = 0.096$) are collected for two flow-through times after reaching a quasi-steady state for integrated heat release rate. Four axial stations used for spray properties comparison with reacting spray measurements [11] are shown in Fig. 7. Figs. 8 and 9 show a comparison of the measurements and results of the LES computations of the droplet radial velocities and axial velocities as a function of radial distance (Y) at the four axial stations defined by the axial distance (Z). The radial and the axial velocities from the experiment and LES increase with radial distance away from the axis up to a certain radius (Y) and then decrease. The peaks in the radial and the axial velocity profiles shift farther away from the centerline at increasing axial distances as the spray cone angle increases at increasing downstream distances from the nozzle exit. The overall trends in the experimental data are captured reasonably by LES simulations for both the A-2 and the C-1 fuel. Fig. 10 shows a comparison of the radial profiles of the measurements of the droplet SMD at four axial stations and the results of the LES computations. The LES results show the expected central hollow cone of the fuel spray. The LES results also show smaller droplets at a 10 mm distance downstream of the nozzle near the hollow cone. As the downstream distance increases, the dispersion and the differences in the drop sizes at different radial locations widens the larger droplets remaining closer to the axis. The LES results show good agreement with experimental data at the downstream locations. The overall differences in radial profiles of SMD observed in experiments at the four locations between the A-2, and the C-1 fuels are reasonably well captured by the

LES simulations. Spray breakup and evaporation processes are captured well by the present Lagrangian spray model for the A-2 and the C-1 fuels. Overall, the results from the LES simulations for SMD, axial, and radial velocity profiles agree well within engineering accuracy with the corresponding experimental data.

Marchese et al. [60] observed that the locations of the maximum OH* intensity and maximum OH concentration coincide with the maximum temperature for methanol combustion. Le et al. [61] compared the OH-PLIF images with OH* chemiluminescence images for a diesel engine and found that the two showed consistent trends for diesel flame development during high-temperature reactions. Literature shows that both OH and OH* are good indicators of heat release rate and reaction zones. For the present work, only OH* chemiluminescence data are available from the experiment, and the present compact kinetic models do not explicitly include OH* and its pathways. As a result, the line of sight averaged OH from simulations is compared with OH* chemiluminescence from experiments in Fig. 11 for qualitative assessment and to highlight the zones of high-temperature reactions within the combustor. The OH mass fractions from the simulations are first time-averaged over two flow-through periods, and then space averaged. The top row shows the planar cross-sectional OH* chemiluminescence images, and the bottom row shows the line of sight averaged OH mass fraction from LES simulations. The experimental findings for the OH* radical reveal that the A-2 fuel has a more asymmetric distribution than the C-1 fuel. The numerical simulations show a nearly axisymmetric distribution for A-2 and C-1 fuels. The experimentally observed peak locations within the shear layers are reasonably captured in the results of the present LES simulations. The numerical simulations also captured the flame anchoring locations and the flame spread in both the radial and axial directions.

Fig. 12 shows the time-averaged temperature contours on the mid-plane of the combustor ($X = 0$) for both fuels at the stable flame condition ($\varphi = 0.096$) near LBO. These contours reveal the qualitative differences between flame shape and size resulting from the A-2 and C-1 fuels. A closer observation of the temperatures in the primary zone indicates higher temperatures for A-2 fuel than C-1 fuel. The combustion process weakens quickly for C-1 compared to A-2, with a decrease in the equivalence ratio. The flame stabilization is in the region closest to the swirler, and this region is smaller and sharp for C-1, whereas A-2 has a slightly broader annular stabilization region. Although the heat of combustion is slightly higher for the C-1 fuel, the computed peak temperature is 60 K lower for C-1 fuel compared to the A-2 fuel. The

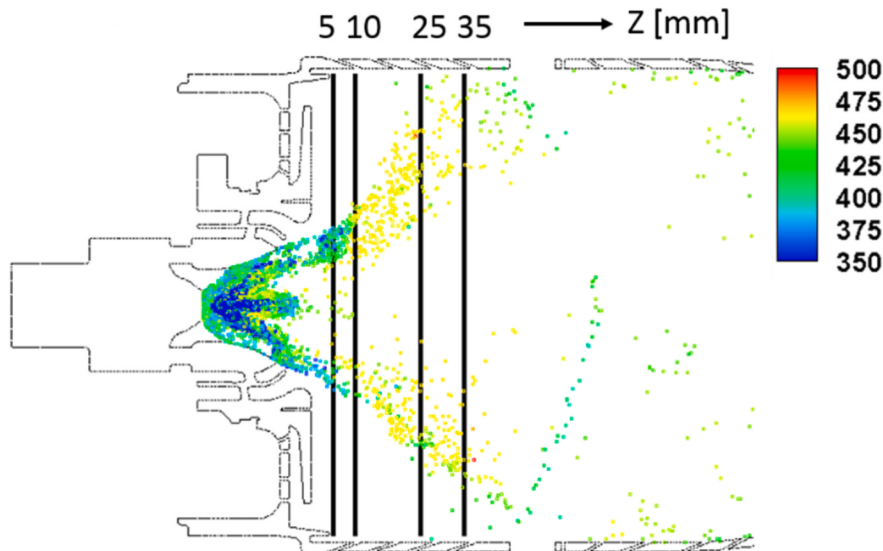


Fig. 7. Axial locations used for comparison of spray statistics on the combustor mid-plane are represented ($X = 0$). The scatter shows fuel particles tagged by a color corresponding to their temperature [K]. (For interpretation of the references to color in this figure legend, the reader is referred to the Web version of this article.)

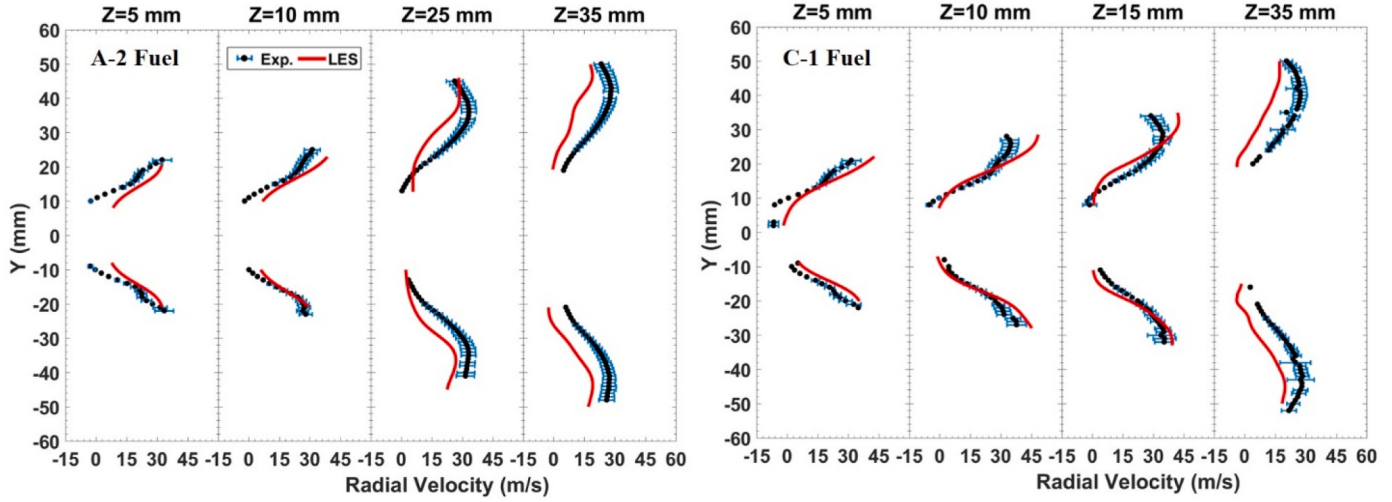


Fig. 8. The comparison of predictions for droplet radial velocity profiles with PDPA measurements [11] for a stable flame at $\varphi = 0.096$.

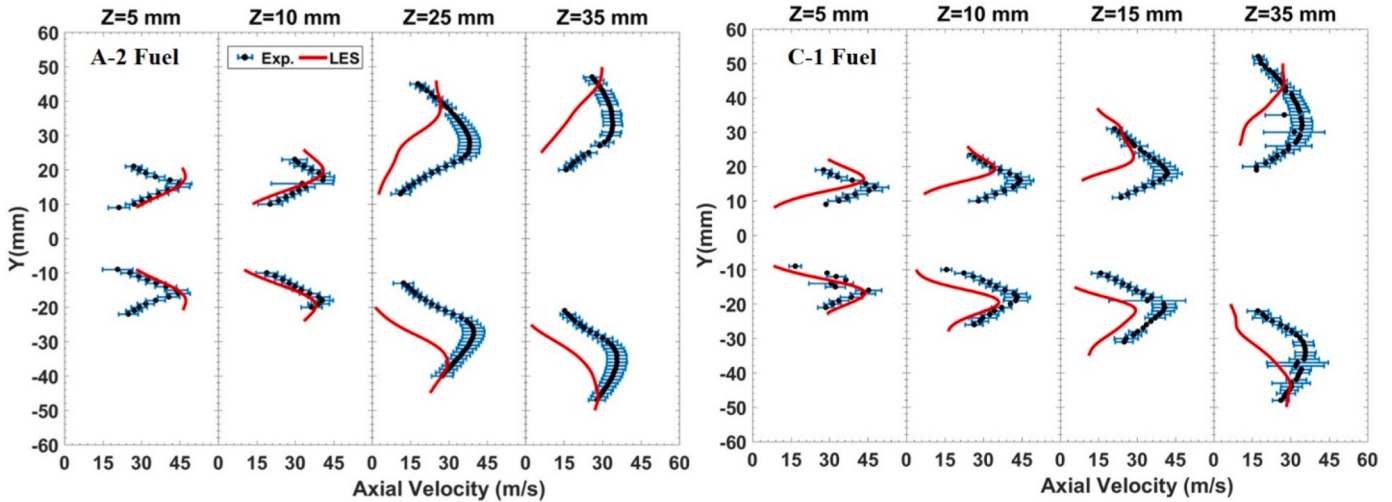


Fig. 9. The comparison of predictions for droplet axial velocity profiles with PDPA measurements [11] for a stable flame at $\varphi = 0.096$.

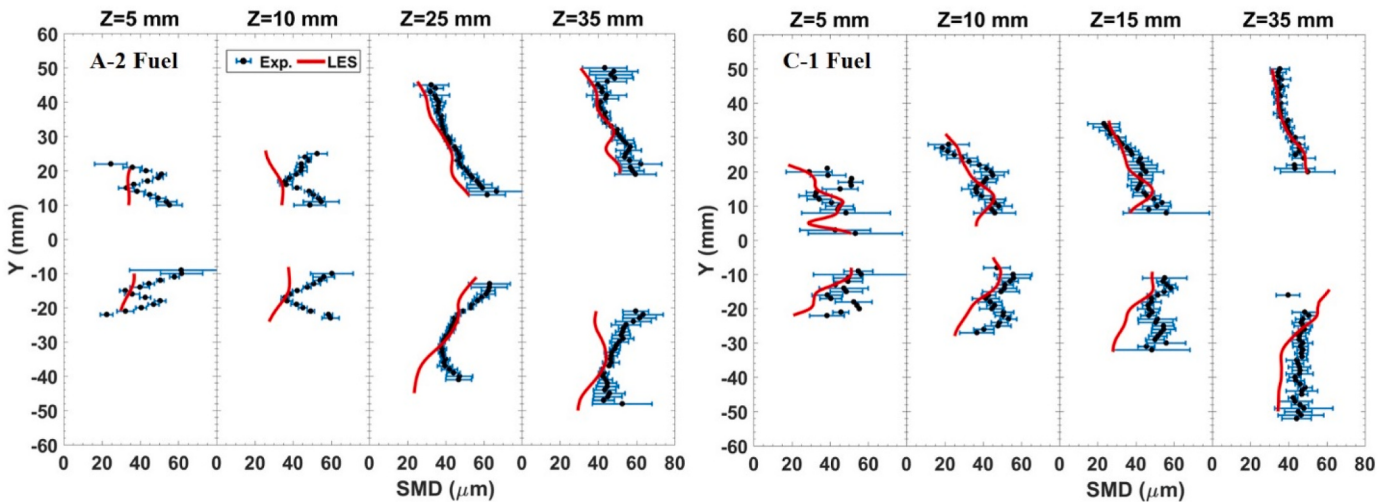


Fig. 10. Comparison of predictions for droplet SMD profiles with PDPA measurements [11] for a stable flame at $\varphi = 0.096$.

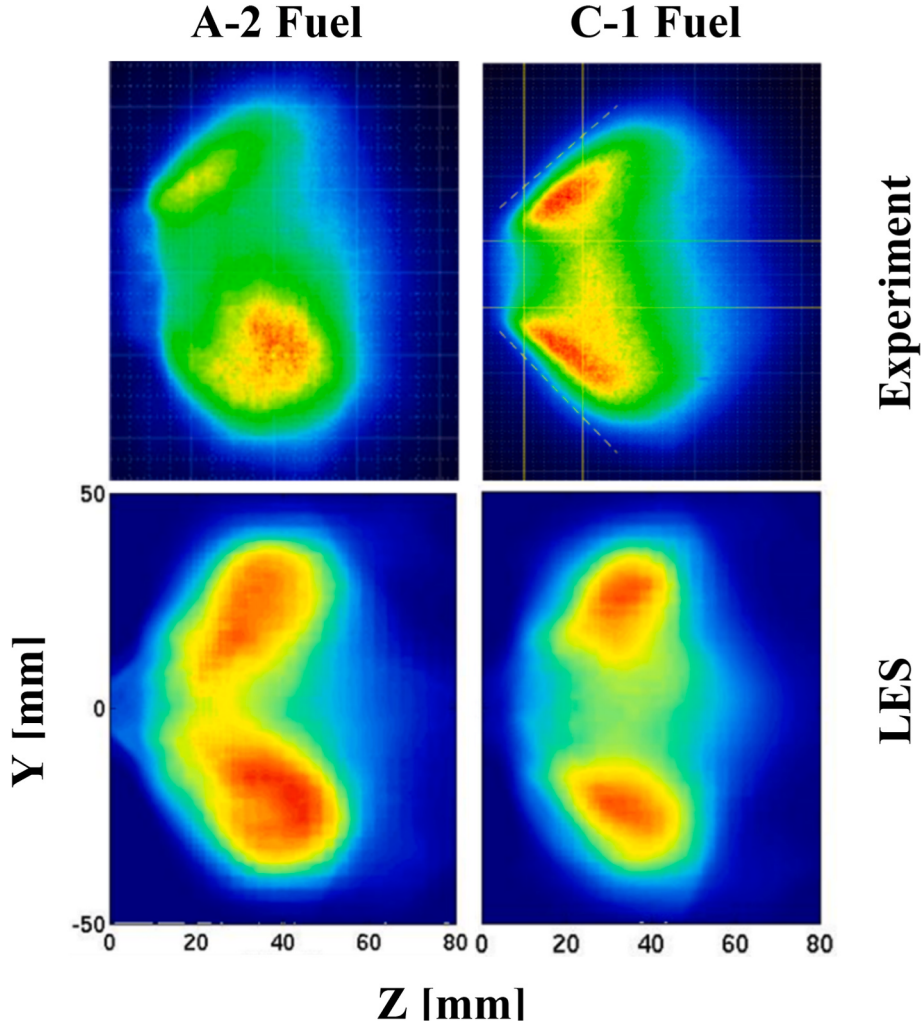


Fig. 11. A qualitative comparison of OH^* chemiluminescence images [11] with line-of-sight averaged OH mass fraction from LES simulations for A-2 and C-1 fuels.

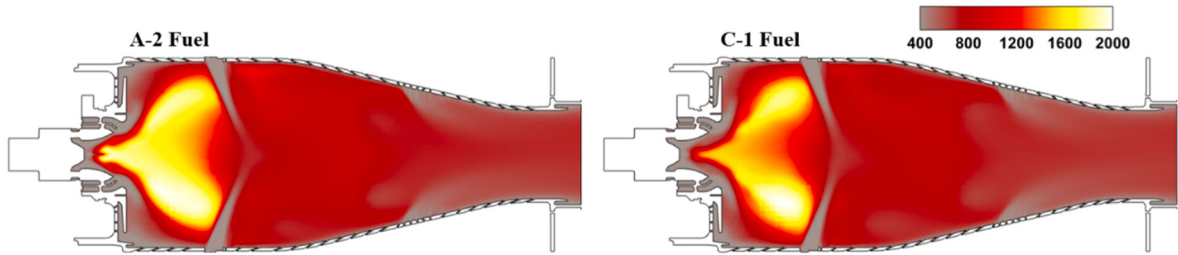


Fig. 12. Comparison of time-averaged temperature [K] on the mid-plane ($X = 0$) for A-2 and C-1 fuels at the stable flame condition ($\varphi = 0.096$) near LBO.

computed temperature field is consistent with a 35% reduction in the measured photodiode intensities between A-2 and C-1 fuels [4].

4.2. Computations of fuel sensitivity to LBO

The computations of fuel sensitivity to LBO for A-2 and C-1 fuels are discussed in this section. The LBO simulations are carried out by progressively reducing the fuel flow rate from the stable flame condition at $\varphi = 0.096$ in a stepwise manner until the flame blows out. The flame condition is monitored by tracking the volume integrated total heat release rate in the combustor. Fig. 13 shows the total heat release rate evolution within the combustor from stable flame condition to LBO for both A-2 (left) and C-1 (right) fuels. First, the global equivalence ratio is

lowered to 0.090 from 0.096 for A-2 fuel, and then the simulations are continued until the total heat release rate reaches a quasi-steady state again. Then, the equivalence ratio is further reduced to 0.085. The flame is stable for a few milliseconds, after which the heat release rate drastically decreases towards zero, showing that $\varphi = 0.085$ defines the flame blowout. A similar approach is followed for the C-1 fuel. The experiments have shown that the flames fueled by the C-1 fuel blow out at a higher equivalence ratio than the equivalence ratio at which the flames fueled with the A-2 fuel. This necessitates smaller steps in the fuel flow reduction to accurately predict the global equivalence ratio at LBO for the C-1 fuel. Therefore, the global equivalence ratio is first decreased from 0.096 to 0.094, and the simulations are continued until the total heat release rate reaches a quasi-steady state. Then, the equivalence

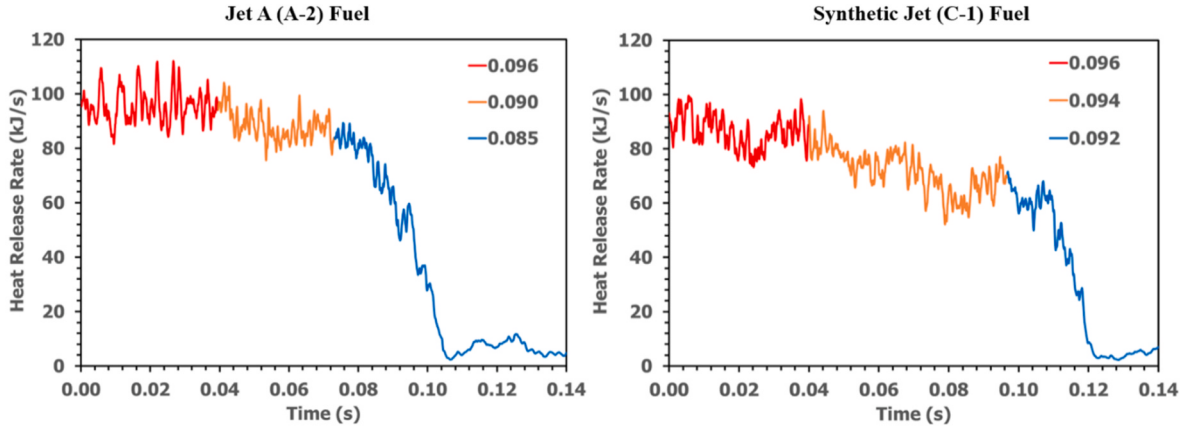


Fig. 13. Volume integrated heat release rate during the LBO for A-2 and C-1 fuels.

ratio is further reduced to 0.092. The heat release rate for the flames with the C-1 fuel falls sharply at the equivalence ratio of 0.092 and flame blows out. In simulations, C-1 fuel blow out at a higher equivalence ratio than the A-2 fuel. This is consistent with the behavior observed in the combustor experiments. A comparison of the trends in the experimental data and the results of the LES simulations for the relative behavior of the C-1 and A-2 with regards to LBO is shown in Fig. 14. The LES simulations with the compact kinetic mechanisms developed in this study successfully predicted the LBO for the two fuels.

An analysis of the evolution of the flame structure during the LBO process based on the changes in the distribution of temperatures and OH radical concentrations across the combustor mid-plane was considered. Fig. 15 shows the instantaneous temperature distributions within the combustor mid-plane ($X = 0$) for A-2 (left) and C-1 (right) fuels with varying fuel flow rates towards LBO. The predicted instantaneous mass fractions of OH radical within the flames fueled by A-2 and C-1 with varying fuel flow rates are shown in Fig. 16. The instantaneous temperature distributions clearly show that the flames with the A-2 fuel result in higher heat release rates and higher temperatures compared to the flames with the C-1 fuel. The rapid mixing of the primary zone gases with the flows of the dilution and effusion cooling air reduces the temperature to ~ 1000 K in the combustor section downstream of the first row of dilution jets. The flame is stable with higher temperatures in the

central recirculation zones (CRZ) within the primary zone of the combustor for both fuels at the baseline condition corresponding to $\varphi = 0.096$. As the fuel flow rate is reduced from the baseline stable condition, the temperature and the size of the areas of intense burning are reduced in the recirculation zones for both fuels. The C-1 fuel show greater reductions in temperature and OH concentration compared to A-2. This is also clearly seen from the contours of the OH mass fraction in Fig. 16 for the two fuels. The higher mass fractions of OH radical in the primary zone indicate larger high-temperature diffusion flames. The A-2 fuel shows a relatively stronger root at the stable flame conditions compared to the root of the flame fueled by the C-1 fuel. The A-2 fuel shows a thinner OH zone with a reduced equivalence ratio and a corresponding decrease in the recirculation zone temperature before flame blows out at $\varphi = 0.085$. A similar phenomenon is observed for the flames with the C-1 fuel before the LBO at $\varphi = 0.092$. The flame fueled by the C-1 fuel blows out at a higher equivalence ratio because of the lower burning rates at the stable baseline conditions and significantly higher reduction in the OH concentration and recirculation temperature compared to the flame with the A-2 fuel. The lower reaction rates associated with the reduced fuel flow rate significantly decreased the concentration of OH radicals, reduced the temperature of the recirculating gases, and thereby destabilized the flame root and finally led to a global flame extinction (LBO).

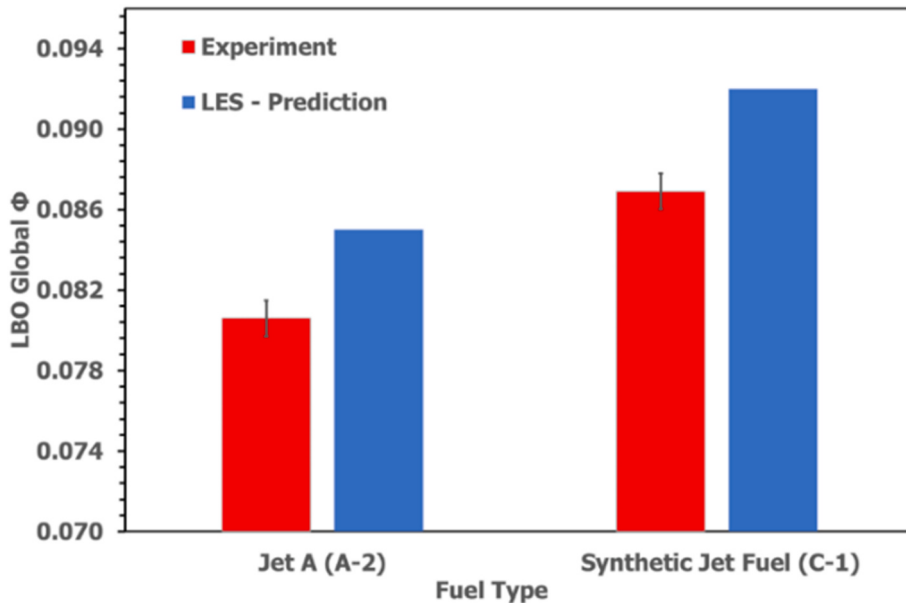


Fig. 14. Comparison of the predicted global LBO equivalence ratio with experiment [4] for A-2 and C-1 fuels.

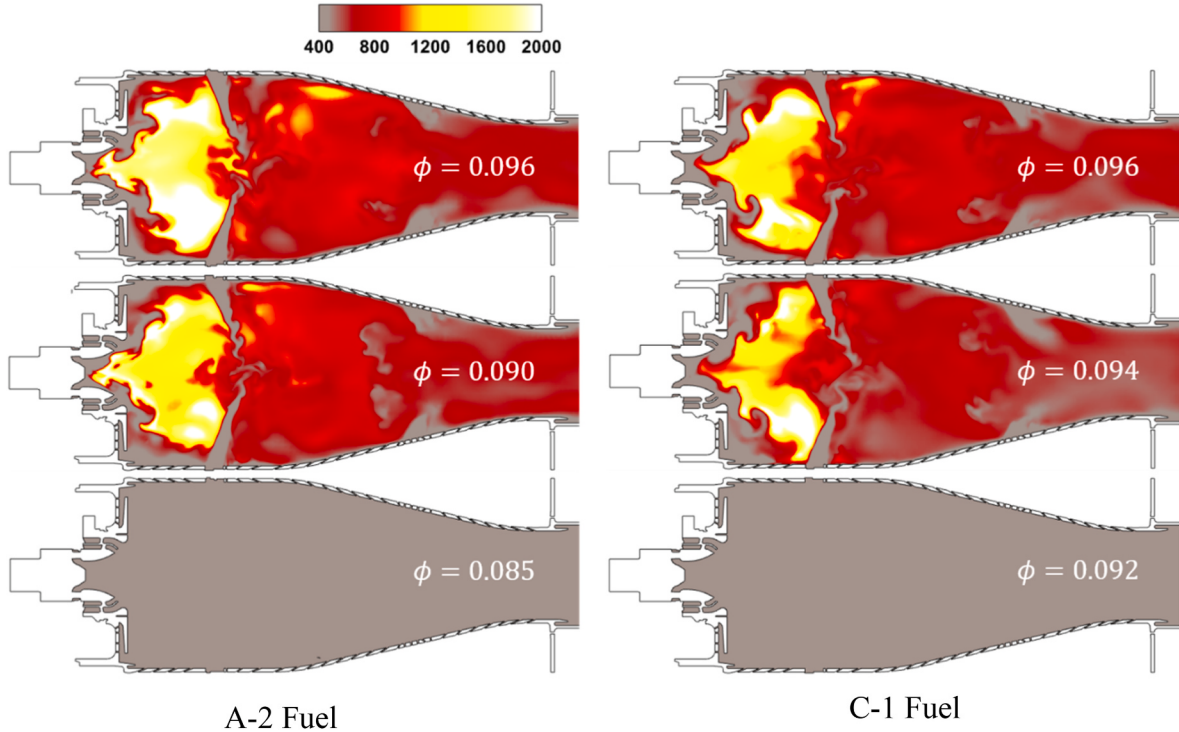


Fig. 15. Contours of instantaneous temperature [K] on the combustor mid-plane for A-2 and C-1 fuels during the LBO process.

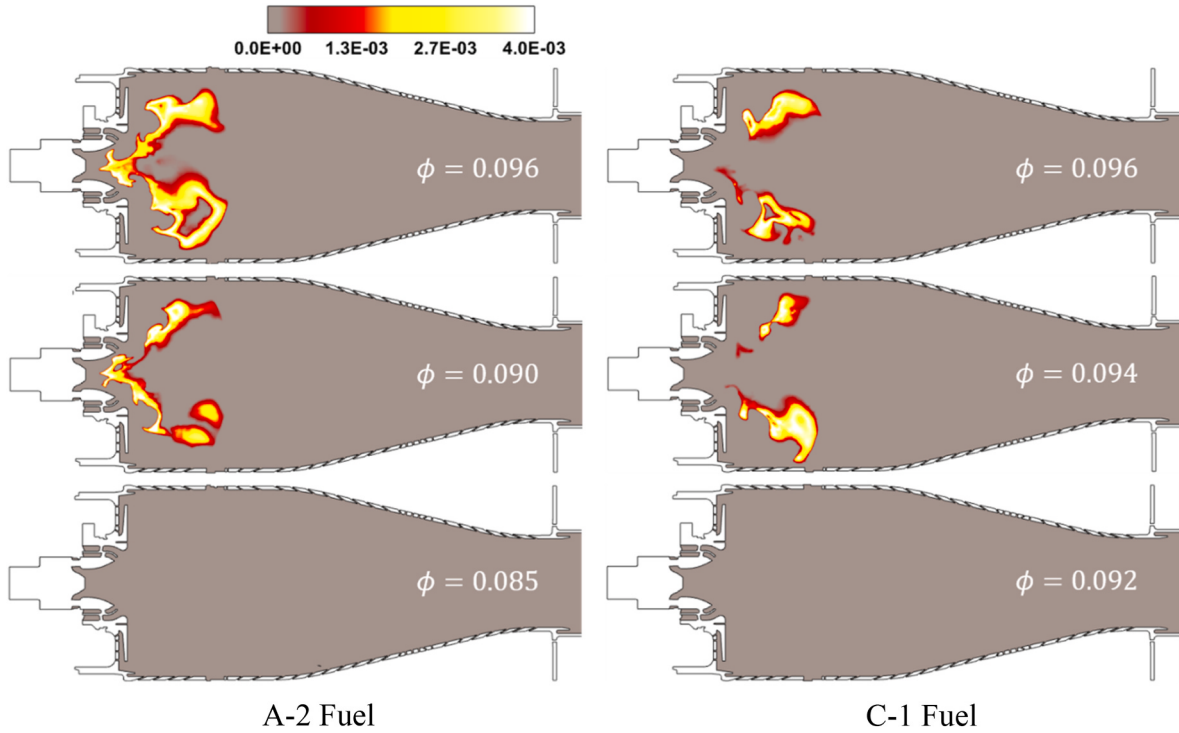


Fig. 16. Instantaneous mass fraction of OH distribution with changing fuel flow rate for A-2 and C-1 fuels.

These processes associated with the complex behavior of flames fueled by A-2 and C-1 fuels are well captured by the present LES simulations. The LBO trends are accurately computed, with the prediction of individual LBO equivalence ratios within 5.5% and 5.9% for the flames with A-2 and C-1 fuels, respectively. Considering the challenges of the physicochemical processes in such a complex, realistic combustor configuration, the agreement between the results of the computations

and the experiments is satisfactory. The autonomous and adaptive meshing-based LES simulations employing the newly developed compact kinetic mechanisms predicted the fuel sensitivity to LBO trends very well.

5. Summary and conclusions

A comprehensive computational methodology is developed to compute the fuel sensitivity to Lean Blowout (LBO) in a practical gas turbine combustor operating at engine-relevant conditions. The computational domain of the combustor consists of all the complex flow passages as present in the real combustor. The airflow through thousands of tiny effusion holes on the combustor and the dome liners is resolved in the simulations. An autonomous and adaptive meshing is employed to generate and adapt the mesh on the fly based on the local velocity, temperature, and species concentration gradients to accurately resolve the flow and flame features. Novel compact kinetic mechanisms based on fuel surrogates are developed, validated, and implemented successfully for conventional (A-2) and alternative (C-1) jet fuels in the CFD solver for the first time. Fuel spray is modeled using the multi-ring injection with boundary conditions derived from PDPA measurements to accurately represent the realistic hollow cone spray observed in the experiments. The simulations are first performed for the stable combustion corresponding to a global equivalence ratio of 0.096 near LBO. The flame shape and spray statistics are validated with experiments at this stable flame condition. The flame anchoring location and flame spread in the axial and radial direction are well captured in the simulations.

The computed spray statistics at this stable flame condition for the SMD, droplet axial, and radial velocities are in reasonable agreement with reacting spray measurements considering the geometric complexity. Simulations are completed, similar to the experiments, by progressively reducing the fuel flow rate until the flame blowout. The simulations are run for each reduction in the fuel flow rate until a quasi-steady state is reached for integrated heat release rate. The volume integrated total heat release is used to monitor the flame health and blowout process. The estimated global equivalence ratio at blowout for A-2 fuel is 0.085 and for C-1 fuel is 0.092. These high-fidelity numerical simulations with newly developed kinetic mechanisms accurately predict the fuel sensitivity to LBO trends between conventional and alternative jet fuels. The predictions agree with the experimental data within ~6% uncertainty. The qualitative analysis of the flame structure reveals that the alternative fuel shows weak burning even at the same equivalence ratio corresponding to stable combustion near the LBO and therefore blows out at a higher equivalence ratio compared to the flames fueled with the conventional fuel. The recirculating gas temperature plays an essential role in maintaining the required evaporation rates and heat release rates for a stable flame. A successful demonstration of the computational methodology for a practical combustor enables to compute the figures of merit for alternative fuels reliably. It helps reduce the number of laboratory tests and hence saves significant costs associated with the fuel certification process.

Declaration of competing interest

The authors declare that they have no known competing financial interests or personal relationships that could have appeared to influence the work reported in this paper.

Acknowledgments

The financial support from the NASA Tools and Transformational Technologies (TTT) program with award number NNX15AU91A is acknowledged. The Bilsland Dissertation Fellowship from the Graduate School at Purdue University is acknowledged. The research aide received from Argonne National Laboratory with financial support from the U.S. Department of Energy under contract no. DE-AC02-06CH11357 is acknowledged. Convergent Science provided the licenses and technical support for this work. The HPC resources at NASA HECC and Laboratory Computing Resource Center at Argonne National Laboratory are appreciated. We acknowledge the NJFCP program and the members

of the computational subgroup for sharing the computational domain, the boundary conditions, the experimental data, and for many technical discussions.

The compact models and surrogate formulation approach used in this study were developed under support from subcontract No. SB1503-001-1 as part of a NASA Small Business Innovative Research (SBIR) Phase II Award (NASA Prime NNX15CC23C) to Spectral Energies LLC, Dayton, OH and by Subcontract 15-7900-0006-03-C1 as part of an Air Force Contract (FA8650-14-D-241) to Universal Technology Corporation, Dayton, OH.

References

- [1] M. Colket, J. Heyne, M. Rumizen, M. Gupta, T. Edwards, W.M. Roquemore, G. Andac, R. Boehm, J. Lovett, R. Williams, J. Condevaux, D. Turner, N. Rizk, J. Tishkoff, C. Li, J. Moder, D. Friend, V. Sankaran, Overview of the national jet fuels combustion program, *AIAA J.* (2017), <https://doi.org/10.2514/1.J055361>.
- [2] J.S. Heyne, M.B. Colket, M. Gupta, A. Jardines, J.P. Moder, J.T. Edwards, M. Roquemore, C. Li, M. Rumizen, Year 2 of the National Jet Fuels Combustion Program: towards a Streamlined Alternative Jet Fuels Certification Process, 55th AIAA Aerospace Sciences Meeting, 2017, pp. 1–14, <https://doi.org/10.2514/6.2017-0145>.
- [3] J.R. Monfort, S. Stouffer, T. Hendershott, P. Wrzesinski, W. Foley, K.D. Rein, Evaluating Combustion Instability in a Swirl-Stabilized Combustor Using Simultaneous Pressure, Temperature, and Chemiluminescence Measurements at High Repetition Rates, *55th AIAA Aerospace Sciences Meeting* (January), 2017, pp. 1–12, <https://doi.org/10.2514/6.2017-1101>.
- [4] S. Stouffer, T. Hendershott, J.R. Monfort, J. Diemer, E. Corporan, P. Wrzesinski, A. W. Caswell, Lean Blowout and Ignition Characteristics of Conventional and Surrogate Fuels Measured in a Swirl Stabilized Combustor, *55th AIAA Aerospace Sciences Meeting* (January), 2017, pp. 1–14, <https://doi.org/10.2514/6.2017-1954>.
- [5] R.D. Stachler, J.S. Heyne, S.D. Stouffer, J.D. Miller, W.M. Roquemore, Investigation of combustion emissions from conventional and alternative aviation fuels in a well-stirred reactor, in: Submitted to the 55th AIAA Aerospace Sciences Meeting (January), 2017, pp. 1–28, <https://doi.org/10.2514/6.2017-0382>.
- [6] E. Corporan, J.T. Edwards, S. Stouffer, M. DeWitt, Z. West, C. Klingshirn, C. Bruening, Impacts of Fuel Properties on Combustor Performance, Operability and Emissions Characteristics, *55th AIAA Aerospace Sciences Meeting* (January), 2017, pp. 1–19, <https://doi.org/10.2514/6.2017-0380>.
- [7] T. Buschhagen, R.Z. Zhang, A.J. Bokhart, R.M. Gejji, S.V. Naik, R.P. Lucht, J. P. Gore, P.E. Sojka, C.D. Slabaugh, S. Meyer, Effect of Aviation Fuel Type and Fuel Injection Conditions on Non-reacting Spray Characteristics of a Hybrid Airblast Fuel Injector, *54th AIAA Aerospace Sciences Meeting* (January), 2016, pp. 1–18, <https://doi.org/10.2514/6.2016-1154>.
- [8] T.H. Hendershott, S. Stouffer, J.R. Monfort, J. Diemer, K. Busby, E. Corporan, P. Wrzesinski, A.W. Caswell, Ignition of conventional and alternative fuel at low temperatures in a single-cup swirl-stabilized combustor, in: 2018 AIAA Aerospace Sciences Meeting. American Institute of Aeronautics and Astronautics, 2018, <https://doi.org/10.2514/6.2018-1422>.
- [9] A. Bokhart, D. Shin, N.S. Rodrigues, P. Sojka, J.P. Gore, R.P. Lucht, Spray characteristics of a hybrid airblast pressure-swirl atomizer at near lean blowout conditions using phase Doppler anemometry, in: 2018 AIAA Aerospace Sciences Meeting. American Institute of Aeronautics and Astronautics, 2018, <https://doi.org/10.2514/6.2018-2187>.
- [10] A. Bokhart, D. Shin, R.M. Gejji, P. Sojka, J.P. Gore, R.P. Lucht, S.V. Naik, T. Buschhagen, Spray measurements at elevated pressures and temperatures using phase Doppler anemometry, *55th AIAA Aerospace Sciences Meeting*, American Institute of Aeronautics and Astronautics, 2017, <https://doi.org/10.2514/6.2017-0828>.
- [11] E. Mayhew, C.M. Mitsingas, B. McGann, T. Hendershott, S. Stouffer, P. Wrzesinski, A.W. Caswell, T. Lee, Spray Characteristics and Flame Structure of Jet A and Alternative Jet Fuels, *55th AIAA Aerospace Sciences Meeting*, 2017, <https://doi.org/10.2514/6.2017-0148>.
- [12] J.T. Edwards, Reference Jet Fuels for Combustion Testing, *55th AIAA Aerospace Sciences Meeting*, 2017, pp. 1–58, <https://doi.org/10.2514/6.2017-0146>.
- [13] T. Lieuwen, V. McDonell, E. Petersen, D. Santavicca, Fuel flexibility influences on premixed combustor blowout, flashback, autoignition, and stability, *J. Eng. Gas Turbines Power* 130 (1) (2008) 11506–11510.
- [14] M. Stöhr, I. Boxx, C. Carter, W. Meier, Dynamics of lean blowout of a swirl-stabilized flame in a gas turbine model combustor, *Proc. Combust. Inst.* 33 (2) (2011) 2953–2960, <https://doi.org/10.1016/j.proci.2010.06.103>.
- [15] L. Esclapez, P.C. Ma, E. Mayhew, R. Xu, S. Stouffer, T. Lee, H. Wang, M. Ihme, Fuel effects on lean blow-out in a realistic gas turbine combustor, *Combust. Flame* 181 (2017) 82–99, <https://doi.org/10.1016/j.combustflame.2017.02.035>.
- [16] H. Wang, R. Xu, K. Wang, C.T. Bowman, R.K. Hanson, D.F. Davidson, K. Brezinsky, F.N. Egolfopoulos, A physics-based approach to modeling real-fuel combustion chemistry - I. Evidence from experiments, and thermodynamic, chemical kinetic and statistical considerations, *Combust. Flame* (2018), <https://doi.org/10.1016/j.combustflame.2018.03.019>.
- [17] R. Xu, K. Wang, S. Banerjee, J. Shao, T. Parise, Y. Zhu, S. Wang, A. Movaghfar, D. J. Lee, R. Zhao, X. Han, Y. Gao, T. Lu, K. Brezinsky, F.N. Egolfopoulos, D. F. Davidson, R.K. Hanson, C.T. Bowman, H. Wang, A physics-based approach to

- modeling real-fuel combustion chemistry – II. Reaction kinetic models of jet and rocket fuels, *Combust. Flame* (2018), <https://doi.org/10.1016/j.combustflame.2018.03.021>.
- [18] Y. Tao, R. Xu, K. Wang, J. Shao, S.E. Johnson, A. Movaghfar, X. Han, J.-W. Park, T. Lu, K. Brezinsky, F.N. Egolfopoulos, D.F. Davidson, R.K. Hanson, C.T. Bowman, H. Wang, A Physics-based approach to modeling real-fuel combustion chemistry – III. Reaction kinetic model of JP10, *Combust. Flame* 198 (2018) 466–476, <https://doi.org/10.1016/j.combustflame.2018.08.022>.
- [19] K. Wang, R. Xu, T. Parise, J. Shao, A. Movaghfar, D.J. Lee, J.-W. Park, Y. Gao, T. Lu, F.N. Egolfopoulos, D.F. Davidson, R.K. Hanson, C.T. Bowman, H. Wang, A physics-based approach to modeling real-fuel combustion chemistry – IV. HyChem modeling of combustion kinetics of a bio-derived jet fuel and its blends with a conventional Jet A, *Combust. Flame* 198 (2018) 477–489, <https://doi.org/10.1016/j.combustflame.2018.07.012>.
- [20] S. Dooley, S.H. Won, M. Chaos, J. Heyne, Y. Ju, F.L. Dryer, K. Kumar, C.-J. Sung, H. Wang, M.A. Oehlschlaeger, R.J. Santoro, T.A. Litzinger, A jet fuel surrogate formulated by real fuel properties, *Combust. Flame* 157 (12) (2010) 2333–2339, <https://doi.org/10.1016/j.combustflame.2010.07.001>.
- [21] S. Dooley, S.H. Won, J. Heyne, T.I. Farouk, Y. Ju, F.L. Dryer, K. Kumar, X. Hui, C.-J. Sung, H. Wang, M.A. Oehlschlaeger, V. Iyer, S. Iyer, T.A. Litzinger, R.J. Santoro, T. Malewicki, K. Brezinsky, The experimental evaluation of a methodology for surrogate fuel formulation to emulate gas phase combustion kinetic phenomena, *Combust. Flame* 159 (4) (2012) 1444–1466, <https://doi.org/10.1016/j.combustflame.2011.11.002>.
- [22] S. Dooley, S.H. Won, S. Jahangirian, Y. Ju, F.L. Dryer, H. Wang, M. A. Oehlschlaeger, The combustion kinetics of a synthetic paraffinic jet aviation fuel and a fundamentally formulated, experimentally validated surrogate fuel, *Combust. Flame* 159 (10) (2012) 3014–3020, <https://doi.org/10.1016/j.combustflame.2012.04.010>.
- [23] S. Dooley, S.H. Won, F.M. Haas, J. Santner, Y. Ju, F.L. Dryer, T.I. Farouk, Development of reduced kinetic models for petroleum-derived and alternative jet fuels, in: 50th AIAA/ASME/SAE/ASEE Joint Propulsion Conference 2014, 2014, pp. 1–23, <https://doi.org/10.2514/6.2014-3661>. April 2015.
- [24] F.M. Haas, S.H. Won, F.L. Dryer, Detailed and compact combustion kinetic models for iso-dodecane and Gevo alcohol-to-jet (ATJ) alternative fuel, in: 2016 Spring Technical Meeting of the Eastern States Section of the Combustion Institute, ESSI, 2016, p. 2016.
- [25] Convergent Science Inc, CONVERGE CFD, 2017. Version 2.4, Madison, WI.
- [26] E. Pomraning, Development of Large Eddy Simulation Turbulence Models, University of Wisconsin-Madison, Madison, WI, 2000.
- [27] E. Pomraning, C.J. Rutland, Dynamic one-equation nonviscosity large-eddy simulation model, *AIAA J.* 40 (4) (2002) 689–701, <https://doi.org/10.2514/2.1701>.
- [28] S.K. Jain, S.K. Aggarwal, Compositional effects on the ignition and combustion of low octane fuels under diesel conditions, *Fuel* 220 (2018) 654–670, <https://doi.org/10.1016/j.fuel.2018.02.015>.
- [29] M. Gholamisheeri, I.S. Wichman, E. Toulson, A study of the turbulent jet flow field in a methane fueled turbulent jet ignition (TJI) system, *Combust. Flame* 183 (2017) 194–206, <https://doi.org/10.1016/j.combustflame.2017.05.008>.
- [30] M. Rahimi Boldaji, B. Gaineys, B. Lawler, Thermally stratified compression ignition enabled by wet ethanol with a split injection strategy: a CFD simulation study, *Appl. Energy* 235 (2019) 813–826, <https://doi.org/10.1016/j.apenergy.2018.11.009>.
- [31] Z. Liu, L. Zhou, B. Liu, W. Zhao, H. Wei, Effects of equivalence ratio and pilot fuel mass on ignition/extinction and pressure oscillation in a methane/diesel engine with pre-chamber, *Appl. Therm. Eng.* 158 (2019) 113777, <https://doi.org/10.1016/j.applthermaleng.2019.113777>.
- [32] N.M. Hafiz, M.R.A. Mansor, W.M.F. Wan Mahmood, Simulation of the combustion process for a CI hydrogen engine in an argon-oxygen atmosphere, *Int. J. Hydrogen Energy* 43 (24) (2018) 11286–11297, <https://doi.org/10.1016/j.ijhydene.2018.05.022>.
- [33] L. Chen, J. Pan, H. Wei, L. Zhou, J. Hua, Numerical analysis of knocking characteristics and heat release under different turbulence intensities in a gasoline engine, *Appl. Therm. Eng.* 159 (2019) 113879, <https://doi.org/10.1016/j.applthermaleng.2019.113879>.
- [34] H. Werner, H. Wengle, Large eddy simulation of turbulent flow over and around a cube in a plane channel, in: Proceedings of the Eighth Symposium on Turbulent Shear Flows 2, 1991.
- [35] A.A. Amsden, KIVA-3V, A Block Structured KIVA Program for Engines with Vertical or Canted Valves, Los Alamos National Laboratory Technical Report LA-13313-MS, 1997. Los Alamos National Laboratory Report LA-13313-MS.
- [36] P.K. Senecal, K.J. Richards, E. Pomraning, T. Yang, M.Z. Dai, R.M. McDavid, M.A. Patterson, S. Hou, T. Shethaj, A New Parallel Cut-Cell Cartesian CFD Code for Rapid Grid Generation Applied to in-Cylinder Diesel Engine Simulations, SAE International, 2007, pp. 776–790. Technical Paper 2007-01-0159.
- [37] V.R. Hasti, P. Kundu, G. Kumar, S.A. Drennan, S. Som, J.P. Gore, Numerical simulation of flow distribution in a realistic gas turbine combustor, in: 2018 Joint Propulsion Conference (AIAA 2018-4956), 2018, <https://doi.org/10.2514/6.2018-4956>.
- [38] V.R. Hasti, A. Navarkar, J.P. Gore, A data-driven approach using machine learning for early detection of the lean blowout, *Energy AI* 5 (2021) 100099, <https://doi.org/10.1016/j.egyai.2021.100099>.
- [39] V.R. Hasti, High-performance Computing Model for a Bio-Fuel Combustion Prediction with Artificial Intelligence, Ph.D Thesis, Purdue University Graduate School, 2019, <https://doi.org/10.25394/PGS.11320805.v1>.
- [40] V.R. Hasti, P. Kundu, S. Som, J.P. Gore, Numerical simulations and analysis of the complex turbulent flow field in a realistic gas turbine combustor, *Proc. IMechE Part A: J. Power and Energy* (2021) 1–11, <https://doi.org/10.1177/09576509211063255>, 1063255 In press.
- [41] S.B. Pope, Ten questions concerning the large-eddy simulation of turbulent flows, *New J. Phys.* 6 (2004) 35, <https://doi.org/10.1088/1367-2630/6/1/035>. -35.
- [42] V.R. Hasti, S. Liu, G. Kumar, J.P. Gore, Comparison of Premixed Flamelet Generated Manifold Model and Thickened Flame Model for Bluff Body Stabilized Turbulent Premixed Flame, 2018, <https://doi.org/10.2514/6.2018-0150>, 2018 AIAA Aerospace Sciences Meeting (AIAA 2018-0150).
- [43] V.R. Hasti, G. Kumar, S. Liu, R.P. Lucht, J.P. Gore, Large Eddy Simulation of Pilot Stabilized Turbulent Premixed CH4+Air Jet Flames, 2018, <https://doi.org/10.2514/6.2018-0675>, 2018 AIAA Aerospace Sciences Meeting (AIAA 2018-0675).
- [44] V.R. Hasti, R. Ranjan, Analysis of Flame Structure during Longitudinal Combustion Instability within a High-Pressure Shear Coaxial Single Element Combustor, *Symposium on Thermoacoustics in Combustion: Industry Meets Academia (SoTiC 2021)*, 2021. Munich, Germany.
- [45] V.R. Hasti, P. Kundu, G. Kumar, S.A. Drennan, S. Som, J.P. Gore, A Numerical Study of Flame Characteristics during Lean Blow-Out in a Gas Turbine Combustor, 2018, <https://doi.org/10.2514/6.2018-4955>, 2018 Joint Propulsion Conference (AIAA 2018-4955).
- [46] V.R. Hasti, P. Kundu, G. Kumar, S.A. Drennan, S. Som, S.H. Won, F.L. Dryer, J. P. Gore, Lean Blow-Out (LBO) Computations in a Gas Turbine Combustor, 2018, <https://doi.org/10.2514/6.2018-4958>, 2018 Joint Propulsion Conference (AIAA 2018-4958).
- [47] V.R. Hasti, R.P. Lucht, J.P. Gore, Large eddy simulation of hydrogen piloted CH4/air premixed combustion with CO2 dilution, *J. Energy Inst.* 93 (3) (2020) 1099–1109, <https://doi.org/10.1016/j.joei.2019.10.004>.
- [48] M.E. Feyz, V.R. Hasti, J.P. Gore, A. Chowdhury, M.R. Nalim, Scalar predictors of premixed gas ignition by a suddenly-starting hot jet, *Int. J. Hydrogen Energy* 44 (42) (2019) 23793–23806, <https://doi.org/10.1016/j.ijhydene.2019.07.066>.
- [49] M.E. Feyz, V.R. Hasti, J.P. Gore, M.R. Nalim, Large eddy simulation of hot jet ignition in moderate and high-reactivity mixtures, *Comput. Fluid* 183 (2019) 28–37, <https://doi.org/10.1016/j.compfluid.2019.03.014>.
- [50] M.E. Feyz, V.R. Hasti, J.P. Gore, M.R. Nalim, Analytical and numerical study of near-field ignition of H2/air by injection of hot gas, *Combust. Flame* 219 (2020) 373–383, <https://doi.org/10.1016/j.combustflame.2020.05.016>.
- [51] M.E. Feyz, M.R. Nalim, V.R. Hasti, J.P. Gore, Modeling and analytical solution of near-field entrainment in suddenly started turbulent jets, *AIAA J.* 57 (5) (2019) 1877–1884, <https://doi.org/10.2514/1.J057612>.
- [52] S. Dooley, S.H. Won, F.L. Dryer, Chapter 10 - Surrogate Fuels and Combustion Characteristics of Liquid Transportation Fuels, Computer Aided Chemical Engineering, vol. 45, Elsevier, 2019, pp. 513–602, <https://doi.org/10.1016/B978-0-444-64087-1.00010-3>.
- [53] S.H. Won, P.S. Veloo, S. Dooley, J. Santner, F.M. Haas, Y. Ju, F.L. Dryer, Predicting the global combustion behaviors of petroleum-derived and alternative jet fuels by simple fuel property measurements, *Fuel* 168 (2016) 34–46, <https://doi.org/10.1016/j.fuel.2015.11.026>.
- [54] S.H. Won, F.M. Haas, S. Dooley, T. Edwards, F.L. Dryer, Reconstruction of chemical structure of real fuel by surrogate formulation based upon combustion property targets, *Combust. Flame* 183 (2017) 39–49, <https://doi.org/10.1016/J.COMBUSTFLAME.2017.04.032>.
- [55] S.H. Won, F.M. Haas, A. Tekawade, G. Kosiba, M.A. Oehlschlaeger, S. Dooley, F. L. Dryer, Combustion characteristics of C4 iso-alkane oligomers: experimental characterization of iso-dodecane as a jet fuel surrogate component, *Combust. Flame* 165 (2016) 137–143, <https://doi.org/10.1016/j.combustflame.2015.11.006>.
- [56] D.J. Luning Prak, M.H. Jones, P. Trulove, A.M. McDaniel, T. Dickerson, J. S. Cowart, Physical and chemical analysis of alcohol-to-jet (ATJ) fuel and development of surrogate fuel mixtures, *Energy Fuels* 29 (6) (2015) 3760–3769, <https://doi.org/10.1021/acs.energyfuels.5b00668>.
- [57] S.H. Won, N. Rock, S.J. Lim, S. Nates, D. Carpenter, B. Emerson, T. Lieuwen, T. Edwards, F.L. Dryer, Preferential vaporization impacts on lean blow-out of liquid fueled combustors, *Combust. Flame* 205 (2019) 295–304, <https://doi.org/10.1016/j.combustflame.2019.04.008>.
- [58] N. Rock, I. Chtereck, B. Emerson, S.H. Won, J. Seitzman, T. Lieuwen, Liquid fuel property effects on lean blowout in an aircraft relevant combustor, *J. Eng. Gas Turbines Power* 141 (7) (2019), <https://doi.org/10.1115/1.4042010>.
- [59] S. Dooley, S.H. Won, F.M. Haas, J.S. Santner, Y. Ju, F.L. Dryer, T. Farouk, Development of Reduced Kinetic Models for Petroleum-Derived and Alternative Jet Fuels, American Institute of Aeronautics and Astronautics, 2014, <https://doi.org/10.2514/6.2014-3661>.
- [60] A.J. Marchese, F.L. Dryer, V. Nayagam, R.O. Colantonio, Hydroxyl radical chemiluminescence imaging and the structure of microgravity droplet flames, 1, in: Twenty-Sixth Symposium (International) on Combustion 26, 1996, pp. 1219–1226, [https://doi.org/10.1016/S0082-0784\(96\)80338-9](https://doi.org/10.1016/S0082-0784(96)80338-9).
- [61] M.K. Le, S. Kook, Q.N. Chan, E.R. Hawkes, Comparison between OH* chemiluminescence and OH planar laser-induced fluorescence images in a light-duty optical diesel engine, in: 19th Australasian Fluid Mechanics Conference, 2014. Melbourne, Australia.